International Journal of Research
Available at https://edupediapublications.org/journals
p-ISSN: 2348-6848
e-ISSN: 2348-795X
Volume 03 Issue 17
November 2016

Pv System Integrated with Battery Energy Storage Isolated Dc-Dc Converters Based Pmsm Drive Applications

D Srikanth
M-tech Student Scholar
Department of Electrical & Electronics Engineering,
DVR COLLEGE OF ENGINEERING AND TECHNOLOGY,
Kashipur,kandi,Sangareddy,Medak dist
Telangana, India.
Email:srikanthd214@gmail.com

Kuna Prashant
Assistant Professor
Department of Electrical & Electronics Engineering,
DVR COLLEGE OF ENGINEERING AND TECHNOLOGY
Telangana, India.
Email:kuna.prashant07@gmail.com

Abstract-This paper proposes a new isolated three-port bidirectional dc–dc converter, which uses the minimum number of switches. It contains an inductor–capacitor–inductor (LCL)-resonant circuit to achieve zero-current switching (ZCS) for the main switch. The proposed converter has the advantage of using the least number of switches and soft switching for the main switch, which is realized by using an inductor–capacitor– inductor (*LCL*)-resonant circuit. The converter is capable of interfacing sources of different voltage–current characteristics with PMSM drive. The proposed converter is applied for simultaneous power management of a photovoltaic (PV) system with a battery. The PV system and the battery are connected to the unidirectional port and the bidirectional port of the converter, respectively. A maximum power point tracking (MPPT) algorithm is designed for the PV panel to generate the maximum power when solar radiation is available. A charge and discharge controller is designed to control the battery to either absorb the surplus power generated by the PV panel or supply the deficient power to the PMSM drive and study the characteristics of drive. The simulation results are presented by using Mat lab/Simulink software.

Index Terms—Battery, bidirectional dc–dc converter, isolated converter, multiport converter, photovoltaic (PV), soft switching, zero-current switching (ZCS).

I.INTRODUCTION

As the world population is increasing rapidly, the power demand and the load demand is also increasing rapidly. Renewable energy sources hold a vital role in generating the power and meeting with the load demands. With surplus advantages like low or almost nil harmful emissions, reliability, durability and low maintenance, renewable energy sources are now playing a major role in satisfying the future energy demand. However, owing to few disadvantages like fluctuation in output due to climatic conditions, irradiance, and temperature and so on, renewable energy sources are still under the research area [1-3]. To cope up with the drawbacks batteries are used as storage mechanism for smoothing output power, improving start up transitions and dynamic characteristics, and enhancing the peak power capacity. For this purpose hybrid power system combining PV, battery, etc are being proposed [4-6]. These hybrid power systems have the potential to provide high quality, more reliable and efficient power. Many hybrid power systems with various power electronic converters have been proposed in the literature up to now. However, the main shortcomings of these integrating methods are complex system topology, high count of devices, high power losses, expensive cost, and large size [7]. Integrated multi-port converters are used to interface power sources with storage devices. They have the advantages like less components, lower cost, more compact size, and better dynamic performance. In many cases, at least one energy storage device should be incorporated. For example, in the electric vehicle application, the regenerative energy occurs during acceleration or start up. Therefore, it is very important for the port connected to the energy storage to allow bidirectional power flow. Various kinds of topologies have been proposed due to the advantages of multiport converters [8].

A grid connected system is that which works in with the local utility grid so that when the solar produces more electricity than a house is using the surplus power is fed into the grid. If the house requires more power than what the solar panels are producing then the balance of the electricity is supplied by the utility grid [9]. With a standalone solar system the solar panels are not connected to a grid but instead are used to charge a bank of batteries. This set up is used in areas where no public grid is available. But the growth in solar power systems in the last five years has been in the grid connected systems. Because most people live in areas that are connected to a public grid and stand-alone systems are much, much more expensive than the grid connected systems because the batteries are very dear. A grid connected system needs to synchronise input to the grid [10].

Many multiport converter topologies have been presented in the literature and can be roughly divided into two categories. One is non-isolated type [11] the non-isolated converters are usually derived from the typical buck, boost, or buck–boost topologies and are more compact in size. The other is isolated type [12]–[13]: the isolated converters using bridge topologies and multi winding transformers to match wide input voltage ranges. In this paper, a high step-up three-port dc-dc converter for the hybrid PV/battery system is proposed with the following advantages:

p-ISSN: 2348-6848
e-ISSN: 2348-795X
Volume 03 Issue 17
November 2016

1) High voltage conversion ratio is achieved by using coupled inductors;
2) Simple converter topology which has reduced number of the switches and associate circuits; 3) Simple control strategywhich does not need to change the operation mode after acharging/discharging transition occurs unless the charging voltage is too high; and
4) Output voltage is always regulated at 380V under all operation modes.

The major contribution of this paper is to propose anintegrated three-port converter as a non-isolated alternative other than typical isolated topologies for high step-up three-port applications. The proposed switching strategy allows the converter to be controlled by the same two duty cycles in different operation modes.

II. Topology and Operating Principle of the Proposed Converter:

A. Topology of the Proposed Converter

The circuit diagram of the proposed converter is shown in Fig.1, which consists of a low-voltage-side (LVS) circuit and a high-voltage-side (HVS) circuit connected by a high-frequency transformer. The LVS consists of two ports, an energy storage capacitor Cs, the primary winding of the transformer, and an LCL-resonant circuit consisting of two inductors Lr and Lp and a capacitor Cr, where Lp includes the added inductance Lp1 and the leakage inductance of the transformer L′p. The HVS consists of the secondary winding of the transformer and a full-bridge rectifier implemented with the diodes Ds1 ∼ Ds4. The transformer's turn ratio is defined as: n = Np/Ns, where Np and N s represent the numbers of turns of the primary and secondary windings, respectively. Among the switches, S1 is called the main switch because it not only controls the power generated by the source connected to Port 1 (P1) but also changes the direction of the current flowing through the transformer.

In this paper, the two ports on the LVS are connected to a PV panel and a battery. To simplify the analysis, the proposed converter is analyzed by two separate converters: one is a single-switch LCL-resonant converter, and the other is the battery-related buck and boost converter consisting of L2, S2, and S3.

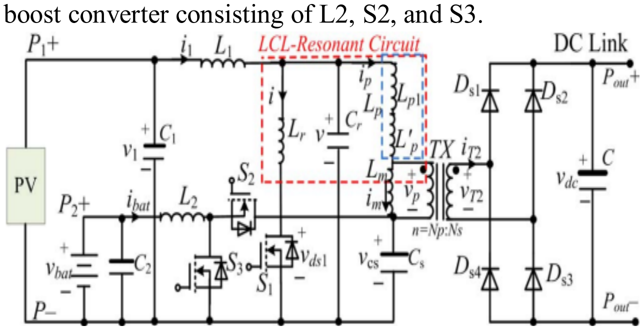

Fig. 1. Proposed isolated three-port bidirectional dc–dc converter for a PV and battery system.

B. Single-Switch LCL-Resonant Converter for PV Panel

In a switching period, the voltages across C1 and Cs can be taken as constant values. Particularly, in the steady state, VCs = V1, where V1 is the output voltage of the PV panel. The converter has seven operating modes depending on the states of the switch S1 and the resonant circuit. Fig.2 shows the equivalent resonant circuit in different modes. The differential equations of the resonant circuit in Mode k (k = 1, . . . , 7) are

$$\begin{cases} v = L_r^{(k)} \cdot \dfrac{di_r^{(k)}}{dt} \\ i_1 = C_r \cdot \dfrac{dv}{dt} + i_r^{(k)} \end{cases} \tag{1}$$

Where v represents the voltage of the capacitor Cr; L (rk) and i(rk) represent the equivalent resonant inductance and the current through the equivalent resonant inductor in the kth

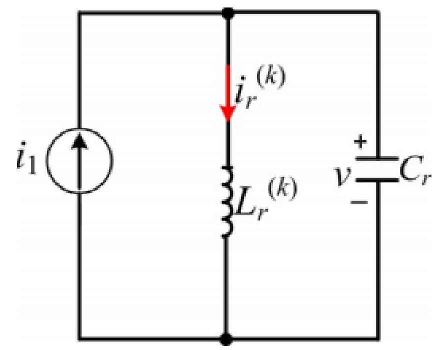

Fig.2. Equivalent resonant circuit.

(k = 1, . . . , 7) operating mode, respectively. Then, v can be solved from (1) and has the following form:

$$v(t)=A^{(k)}\cos\left[\omega^{(k)}(t-t_k)\right]+B^{(k)}\sin\left[\omega^{(k)}(t-t_k)\right]+V^{(k)} \tag{2}$$

Where

$$\omega^{(k)} = \frac{1}{\sqrt{L_r^{(k)} \cdot C_r}} \tag{3}$$

is the resonant frequency in Mode k; V (k) is the particular solution of (1) in Mode k, and A(k) and B(k) are coefficients, which can be expressed as follows:

$$A^{(k)} = v(t_k) - V^{(k)} \tag{4}$$

$$B^{(k)} = \frac{I_1 - i_p(t_k) - i(t_k)}{\omega^{(k)} \cdot C_r} \tag{5}$$

Where v(tk), I1, ip(tk), and i(tk) represent the voltage across Cr and the currents of L1 (i1 can be viewed as a constant value I1 because of a large L1), Lp, and Lr at time tk, respectively. Equations (4) and (5) indicate that

p-ISSN: 2348-6848
e-ISSN: 2348-795X
Volume 03 Issue 17
November 2016

only ω(k) and V (k) are required to determine the parameters of (2).

The steady-state waveforms and equivalent circuits of the seven operating modes of the converter are shown in Figs. 3 and 4, respectively. To facilitate the explanation of the converter operation, define VT = n · Vdc the equivalent output voltage of the converter referred to the primary side of the transformer.

Mode 1—t ∈ [t1, t2] (see Fig.3): Prior to Mode 1, S1 is off; the currents through Lr and Lp are zero and a positive value of I1, respectively, i.e., i(t1) = 0, ip(t1) = I1. When S1 is on, as shown in Fig. 4(a), Lr and Lp resonate with Cr, the current of the inductor Lr increases, and the voltage of the capacitor Cr decreases. Due to the existence of Lr, the current through the switch S1 increases slowly, so that the switch is turned on under a low-di/dt condition. The resonant frequency and the particular solution in this mode can be expressed as follows:

$$\omega^{(1)} = \frac{1}{\sqrt{(L_r//L_p)\cdot C_r}} \tag{6}$$

$$V^{(1)} = \frac{L_r}{L_r+L_p}\cdot(V_1+V_T) \tag{7}$$

Where // represents that Lr and Lp are connected in parallel. In this mode, the current im through the primary magnetizing inductance Lm increases; the current iT2 through the secondary side of the transformer is positive, which indicates the conduction of the Ds1 and Ds3. At the end of Mode 1, ip(t2) = im(t2),i achieves its maximum value Imax, iT(t2) = 0, v(t2) = 0, and vp changes its polarity from positive to negative

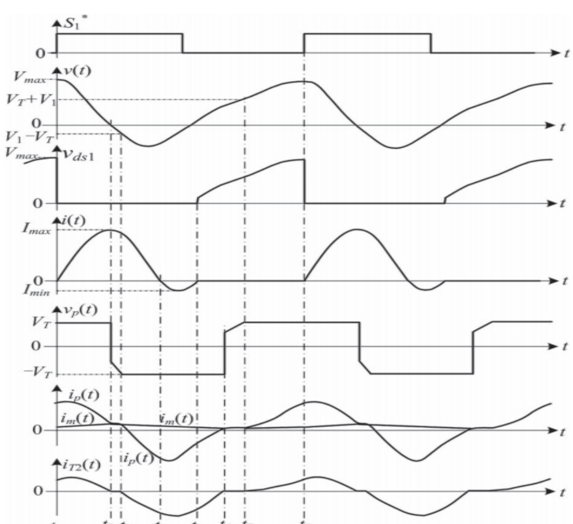

Fig.3.Steady-state waveforms of the proposed converter.

Mode 2—t ∈ [t2, t3]: During which S1 is on, i(t)>0, ip(t)=im(t), and Ds1−Ds4 are reverse biased, such that iT = 0. As shown in Fig. 4(b), Lm, Lp, and Lr resonate with Cr. Since Lm Lp, Lm Lr, then

$$\omega^{(2)} = 1/\sqrt{[(L_p+L_m)//L_r]\cdot C_r} \approx 1/\sqrt{L_r\cdot C_r} \tag{8}$$

$$V^{(2)} = \frac{L_r}{L_r+L_p+L_m}\cdot V \approx \frac{L_r}{L_m}\cdot V_1 \tag{9}$$

At the end of Mode 2, vp(t3) = −VT , v(t3) = V1 − VT , and the diodes Ds2 and Ds4 begin to conduct.

Mode 3—t ∈ [t3, t4]: During which S1 is on, i(t) > 0, vp(t) = −VT , and iT2 < 0. As shown in Fig. 4(c), Lr and Lp resonate with Cr; the energy stored in Lr is released to charge the capacitor Cr; vp is clamped to −VT ; and iT2 is negative, which indicates the conduction of Ds2 and Ds4. Compared to Mode 1, the only difference in the equivalent circuit in this mode is the sign of vp. Thus, ω(3) = ω(1), and

$$V^{(3)} = \frac{L_r}{L_r+L_p}\cdot(V_1-V_T) \tag{10}$$

This mode terminates at time t4 when the current of Lr decreases to zero, i.e., i(t4) = 0.

Mode 4—t ∈ [t4, t5]: During which S1 is on, i(t) < 0, vp(t) = −VT , iT2 < 0, and Ds2 and Ds4 conduct. As shown in Fig.4(d), a negative current flows through the internal diode of the switch S1; the gate signal can be removed to turn off the switch, e.g., at time t5, under the ZCS condition. The circuit equations are the same as those in Mode 3. Thus, ω(4) = ω(1), V (4) = V (3). At the end of Mode 4, i(t5) = 0, and the voltage across the switch S1 is the same as that across the capacitor Cr, i.e., vds1(t5) = v.

Mode 5—t ∈ [t5, t6]: During which S1 is off, i(t) = 0, vp = −VT , and iT2 < 0. As shown in Fig.4(e), Lr and the switch S1 can be neglected in the circuit. The inductor Lp resonates with Cr, and the direction of ip changes from negative to positive. The following can be obtained:

$$\omega^{(5)} = 1/\sqrt{L_p\cdot C_r} \tag{11}$$

$$V^{(5)} = V_1 - V_T \tag{12}$$

At the end of Mode 5, ip(t6) = im(t6), iT2(t6) = 0, and vp changes its polarity from negative to positive.

Mode 6—t ∈ [t6, t7]: During which S1 is off, i(t) = 0, ip(t) = im(t), and Ds1 − Ds4 are reverse biased, such that iT2 = 0. As shown in Fig. 4(f), Lm and Lp resonate with Cr, and Cr is charged. The following can be obtained:

$$\omega_6 = 1/\sqrt{(L_p+L_m)\cdot C_r} \approx 1/\sqrt{L_m\cdot C_r} \tag{13}$$

$$V^{(6)} = V_1. \tag{14}$$

p-ISSN: 2348-6848
e-ISSN: 2348-795X
Volume 03 Issue 17
November 2016

At time t7, v(t7) = V1 + VT and vp(t7) = VT .

Mode 7: t ∈ [t7, t8], during which S1 is off, i(t) = 0, vp(t) = VT , and Ds1 and Ds3 conduct. As shown in Fig.4(g), Lp resonates with Cr, the circuit equations are the same as those in Mode 5 except the sign of vp, then ω(7) = ω(5), and

$$V^{(7)} = V_1 + V_T \tag{15}$$

Once S1 is turned on at time t8, Mode 7 switches to Mode 1. There are five inductances L1, L2, Lr, Lp1, and Lm in the proposed converter that need to be properly designed. Lm is designed based on the following critical inductance Lmc

$$L_{\mathrm{mc}} = \frac{V_T \cdot T}{4 \cdot I_{m,\mathrm{pk}}} \tag{16}$$

Where T is the switching period of the switch S1; Im,pk is the peak current through the magnetizing inductor. In this paper, the root-mean-square (RMS) value of the magnetizing current is designed to be 2% of the RMS value of ip. Then, Lm is designed to be larger than Lmc. Once the transformer is designed, the leakage inductance L′p of the transformer can be measured.Given the load resistance RL and the transformer’s turn ratio n, the quality factor Q of this LCL-resonant converter can be calculated as follows

$$Q = \frac{8 \cdot n^2 \cdot R_L}{\pi^2 \cdot Z} \tag{17}$$

Where Z is the characteristic impedance of the resonant circuit defined as follows:

$$Z = \sqrt{\frac{L_r // \left(L_{p1} + L_p'\right)}{C_r}}. \tag{18}$$

Given the desired value of Q and the value of RL, the value of Z can be calculated from (16). In this paper, Q is selected in the optimal range of [1.5, 5]. Specifically, the value of Q is

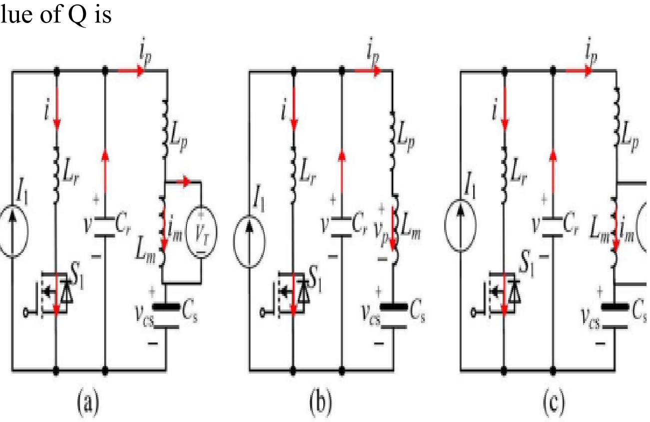

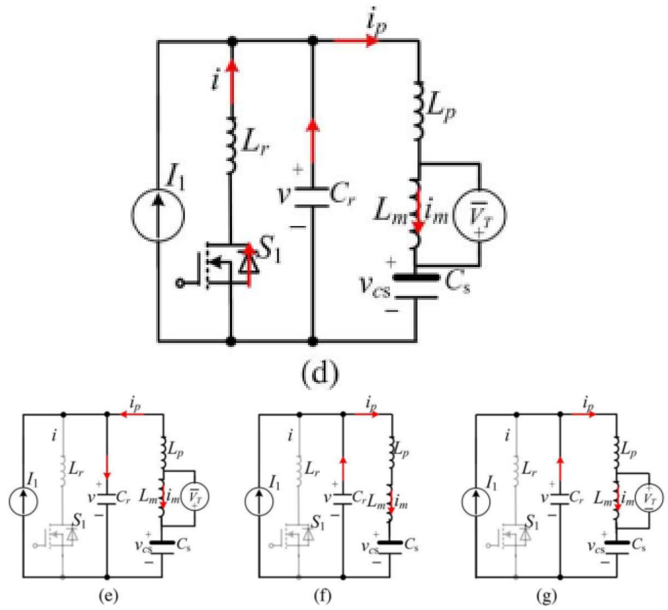

Fig. 4. Equivalent circuits for different operating modes. (a) Mode 1: S1 is on, i > 0, and vp = VT . (b) Mode 2: S1 is on, i > 0, and ip = im. (c) Mode 3: S1 is on, i > 0, and vp = −VT . (d) Mode 4: S1 is being turned off, i < 0, and vp = −VT . (e) Mode 5: S1 is off, i = 0, vp = −VT . (f) Mode 6: S1 is off, i = 0, and I p = im. (g) Mode 7: S1 is off, i = 0, and vp = VT

3.7, when the nominal load is applied. Then, given the resonant frequency, Cr can be calculated from (6) and (18). Considering the necessary condition Lp > Lr to achieve ZCS, Lr = Lp1 is selected, such that the currents through the switch S1 and the transformer are close during the resonant stage. Then, Lr and Lp1 can be calculated from (18) with the measured value of L′p.

The values of L1 and L2 are designed, according to their desired current ripples [10]. In this paper, it is expected that the current ripples are within 5% of their nominal currents.

C. Buck and Boost Converter for Battery

The buck and boost converter consists of the inductor L2, switches S2 and S3, and capacitor Cs. When the generated solar power is larger than the power required by the load, S3 is inactive and S2 is switched on to form the buck converter. Then, the surplus energy generated from the PV panel is stored in the battery. In contrast, when the generated solar power is less than the power required by the load, S2 is switched off and S3 is switched on to form the boost converter. The battery is discharged to Cs to provide the deficient energy required by the load.

III. POWER MANAGEMENT OF THE PROPOSED CONTROLLER

Two controllers are needed to manage the power in the LVS. Their objectives are to regulate the output dc-link voltage to a constant value and manage the power for the two sources, respectively. According to the availability of the solar power, there are three working scenarios of the converter, as illustrated in Fig.5.

A. Three Working Scenarios

Scenario 1 (p1 ≥ pout): the available solar power is more than the load demand. As shown in Fig.5(a), the PV converter works in the MPPT mode; the battery is charged so that the dc-link voltage is controlled at a constant value.

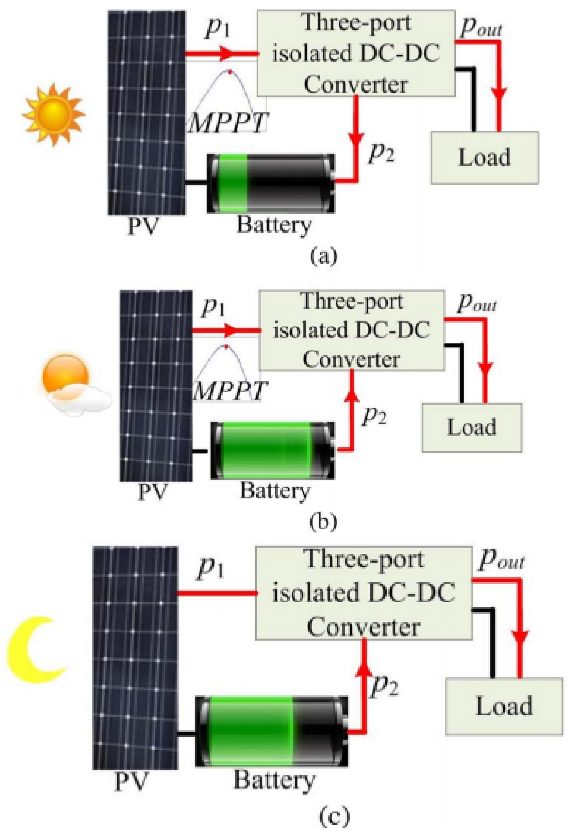

Fig.5. Three working scenarios of the converter (the arrows show the directions of energy flow). (a) Scenario 1 (p1 > pout): PV works in MPPT mode and the battery works in charge mode to absorb the surplus solar energy. (b) Scenario 2 (p1 < pout): PV works in MPPT mode and battery works in discharge mode to provide the deficient energy. (c) Scenario 3 (p1 = 0): there is no solar energy available and battery is discharged to supply load.

Scenario 2 (0 < p1 < pout): there is solar radiation, but the solar power is not sufficient to supply the load. As shown in Fig.5 (b), the PV panel is controlled in the MPPT mode by the MPPT algorithm described later. On the other hand, the deficient power is supplied by the battery, which is discharged by the boost converter, so that the dc-link voltage can be main tained at a constant value.

Scenario 3 (p1 = 0): there is no solar power available and, thus, the battery is discharged to supply the load, as shown in Fig.5(c). The active switches are S1 and S3.

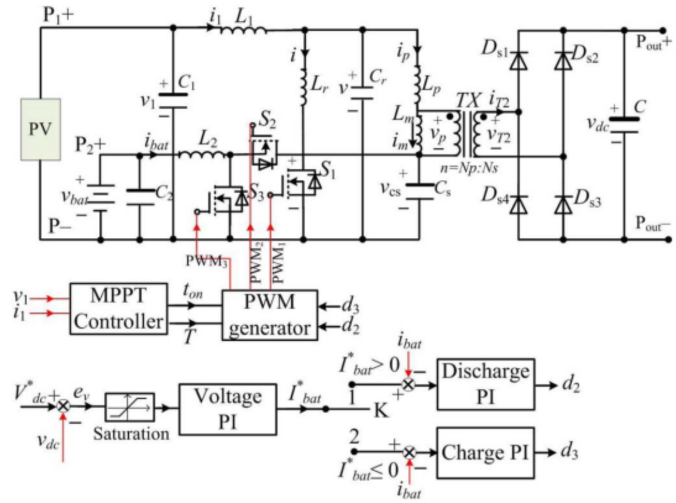

Fig. 6. Overall block diagram of the system with controllers.

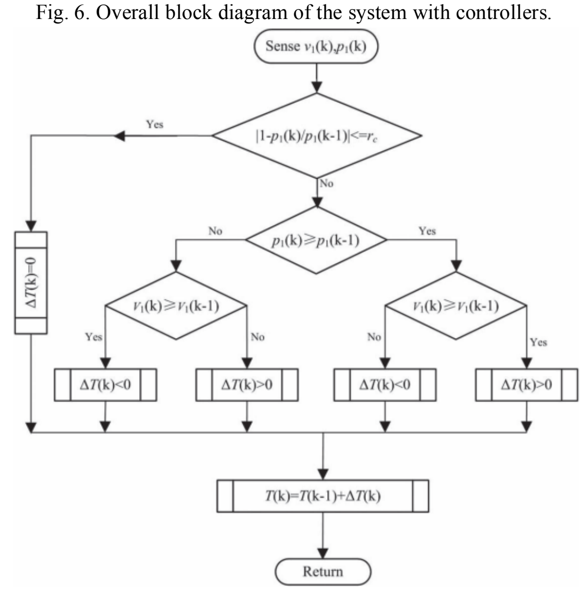

Fig.7. Flowchart of the MPPT algorithm.

Proper controllers are designed to manage the power of the system in different scenarios. Fig.6 shows the overall system with controllers, which include a MPPT controller for the PV panel and charge and discharge controllers for the battery.

B. MPPT Controller for PV Panel

The proposed converter is applied for MPPT control of a PV panel using the perturbation and observation (P&O) MPPT algorithm to maximize the PV panel's output efficiency. Fig.7 shows the flowchart of the MPPT algorithm. A ratio rc is defined to specify the relative power change (RPC) of the PV panel between two consecutive sampling steps. Thus,

p-ISSN: 2348-6848
e-ISSN: 2348-795X
Volume 03 Issue 17
November 2016

$$r_c = \frac{|P_1(k) - P_1(k-1)|}{P_1(k-1)} \quad (19)$$

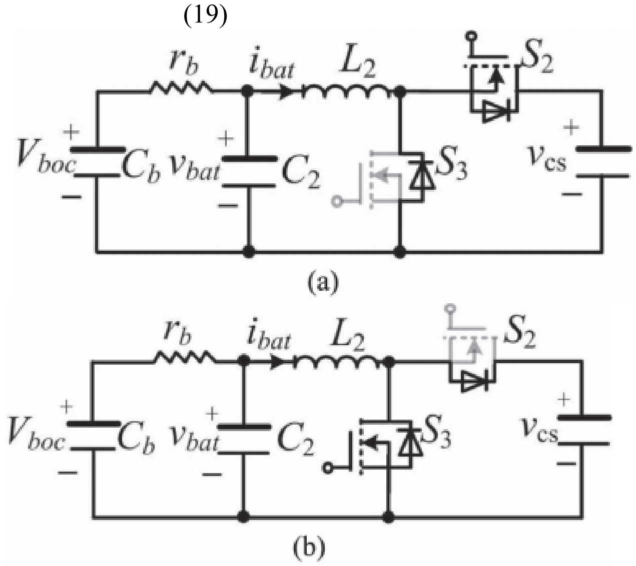

Fig.8. Equivalent circuit of the battery with (a) the buck converter in charge mode and (b) the boost converter in discharge mode.

Where P1(k) and P1(k−1) represent the measured output power of the PV panel in the kth and (k − 1)th steps, respectively.

It can be seen that, for the same power variation value, rc is proportional to 1/P1 (k − 1). In this paper, the switching period (T) will not be changed if the RPC is lower than a predefined value (e.g., 10−4). As shown in Fig. 7, the P&O MPPT algorithm is realized by the frequency modulation method, where the conduction time of S1, i.e., ton, is fixed so that S1 can achieve soft switching.

C. Charge and Discharge Controllers for Battery

Fig. 8(a) and (b) shows the equivalent circuit of the battery and the converter when the battery works in the charge and discharge modes, respectively. To simplify the analysis, the battery is modeled as a capacitor Cb connected in series with its internal resistance rb. Since Cb is sufficiently large, the terminal voltage of the battery, i.e., vbat, can be calculated as Vboc − ibat · rb, where Vboc is the open-circuit voltage of the battery. Then, the transfer function between the battery current ibat and the duty cycle d2 of the switch S2 in the charge mode can be derived as follows:

$$G_c(s) = \frac{i_{\mathrm{bat}}(s)}{d_2(s)} = \frac{(V_1 - V_{\mathrm{bat}}) \cdot \left(s + \frac{1}{r_b \cdot C_2}\right)}{s^2 + \left(\frac{r_2}{L_2} + \frac{1}{r_b \cdot C_2}\right) s + \frac{r_2/r_b + D_2}{L_2 \cdot C_2}} \quad (20)$$

Where V1 and Vbat represent the average voltages of the PV panel and the battery, respectively; r2 and rb represent the parasitic resistance of the inductor L2 and the internal resistance of the battery, respectively; D2 is the steady-state value of the duty cycle of the switch S2.

Similarly, the transfer function between ibat and the duty cycle d3 of the switch S3 in the discharge mode is

$$G_d(s) = \frac{i_{\mathrm{bat}}(s)}{d_3(s)} = \frac{V_1 \cdot \left(s + \frac{1}{r_b \cdot C_2}\right)}{s^2 + \left(\frac{r_2}{L_2} + \frac{1}{r_b \cdot C_2}\right) s + \frac{r_2/r_b + 1}{L_2 \cdot C_2}}. \quad (21)$$

To control the current of the battery, a proportional–integral (PI) controller Kp + Ki/s is used in the charge/discharge mode separately, as shown in Fig.6. Each battery current PI controller takes the current error as the input to generate the duty cycle for S2 or S3 in the charge or discharge mode, respectively. When the reference current I∗bat is zero or negative, the charge PI controller is selected, such that d2 ≥ 0 and d3 = 0. Otherwise, when the reference current I∗bat is positive, the discharge PI controller is selected, such that d3 > 0 and d2 = 0.

The bode plots of ibat(s)/d2(s) and ibat(s)/d3(s) without the PI compensations (i.e., the open-loop transfer functions). The plots imply that the two open loop systems have low gains and 0-dB/dec slopes in the low frequency region. Therefore, the design objective of the PI compensation is to increase the low-frequency gains and make them cross the 0-dB line with a −20-dB/dec slope, while maintaining a sufficiently large phase margin (> 45◦) and a high crossover frequency. By setting the crossover frequency in the range of one to several hundred hertz with a phase margin of 70◦, the charge and discharge PI controllers can be derived. The bode plots of ibat(s)/d2(s) and ibat(s)/d3(s) with the PI compensations (i.e., the closed-loop transfer functions). After the compensations, the low frequency gains have been increased, and the low-frequency slopes are changed to be −20 dB/dec. The crossover frequencies corresponding to the charge and the discharge controllers are 300 Hz and 400 Hz, respectively.

IV Permanent magnet synchronous motors (PMSM)

Permanent magnet synchronous motors (PMSM) are typically used for high-performance and high-efficiency motor drives. High-performance motor control is characterized by smooth rotation over the entire speed range of the motor, full torque control at zero speed, and fast acceleration and deceleration. To achieve such control, vector control techniques are used for PM synchronous motors. The vector control techniques are usually also referred to as field-oriented control (FOC). The basic idea of the vector control algorithm is to decompose a stator current into a magnetic field-generating part and a torque generating part. Both components can be controlled separately after decomposition. Then, the structure of the motor controller (vector control controller) is almost the same as a separately excited DC motor, which simplifies the control of a permanent magnet synchronous motor. Let's start with some basic FOC principles.

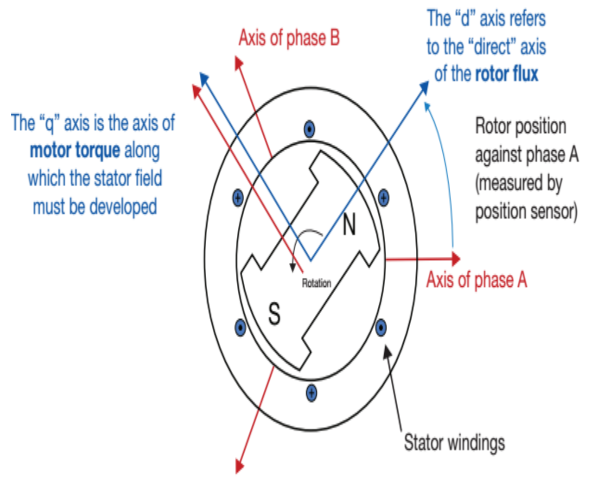

Torque Generation

A reactance torque of PMSM is generated by an interaction of two magnetic fields (one on the stator and one on the rotor). The stator magnetic field is represented by the magnetic flux/stator current. The magnetic field of the rotor is represented by the magnetic flux of permanent magnets that is constant, except for the field weakening operation. We can imagine those two magnetic fields as two bar magnets, as we know a force, which tries to attract/repel those magnets, is maximal, when they are perpendicular to each other. It means that we want to control stator current in such a way that creates a stator vector perpendicular to rotor magnets. As the rotor spins we must update the stator currents to keep the stator flux vector at 90 degrees to rotor magnets at all times. The reactance torque of an interior PM type PMSM (IPMSM) is as follows, when stator and rotor magnetic fields are perpendicular. Torque=32*pp*lPM*I*qs *pp* – Number of pole pairs l PM – Magnetic flux of the permanent magnets *I* qs – Amplitude of the current in quadrature axis As shown in the previous equation, reactance torque is proportional to the amplitude of the q-axis current, when magnetic fields are perpendicular. MCUs must regulate the phase stator current magnitude and at the same time in phase/angle, which is not such an easy task as DC motor control.

How to Simplify Control of Phase Currents to Achieve Maximum Torque

DC motor control is simple because all controlled quantities are DC values in a steady state and current phase/ angle is controlled by a mechanical commentator. How can we achieve that in PMSM control? DC Values/Angle Control First, we need to know the rotor position. The position is typically related to phase A. We can use an absolute position sensor (e.g., resolver) or a relative position sensor (e.g., encoder) and process called alignment. During the alignment, the rotor is aligned with phase A and we know that phase A is aligned with the direct (flux producing) axis. In this state, the rotor position is set to zero (required voltage in d-axis and rotor position is set to zero, static voltage vector, which causes that rotor attracted by stator magnetic field and to align with them [with direct axis]).

1 Three-phase quantities can transform into equivalent two-phase quantities (stationary reference frame) by Clarke transformation.

2. Then, we transform two-phase quantities into DC quantities by rotor electrical position into DC values (rotating reference frame) by Park transformation. The electrical rotor position is a mechanical rotor position divided by numbers of magnetic pole pairs pp. After a control process we should generate three-phase AC voltages on motor terminals, so DC values of the required/generated voltage should be transformed by inverse Park/Clarke transformations.

V.MATLAB/SIMULATION RESULTS

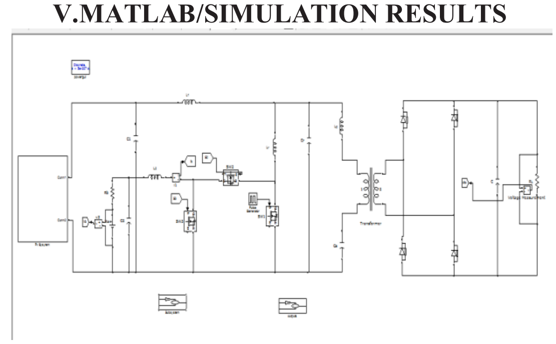

Fig 9Matlab/simulation circuit of isolated three-port bidirectional dc–dc converter for a PV and battery system

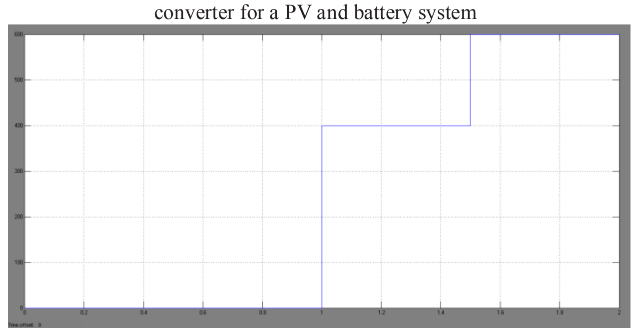

(a)

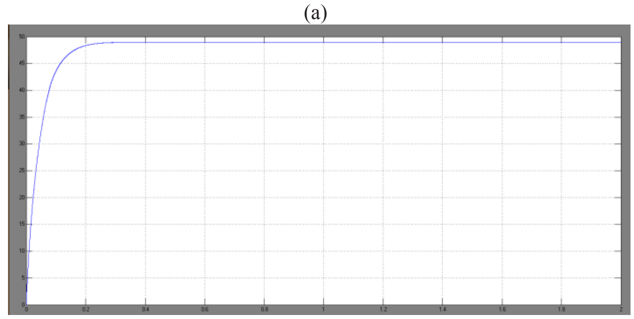

(b)

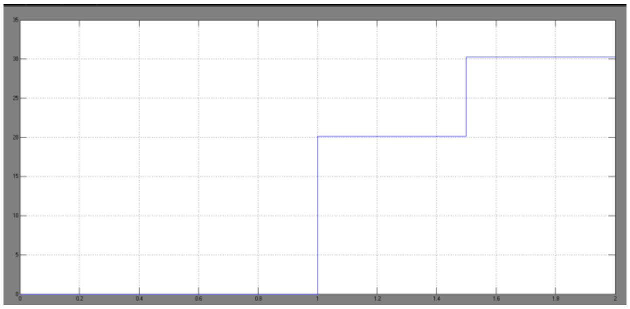

(c)

Fig 10 simulation wave form of step responses: (a) profile of solar radiation, (b) dc-link voltage response, and (c) PV power response.

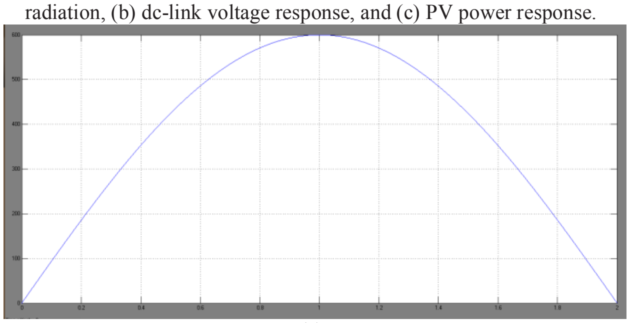

(a)

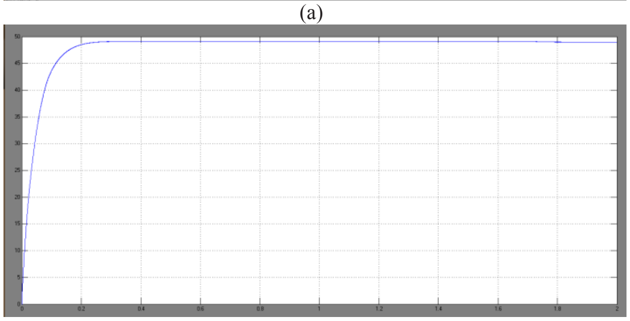

(b)

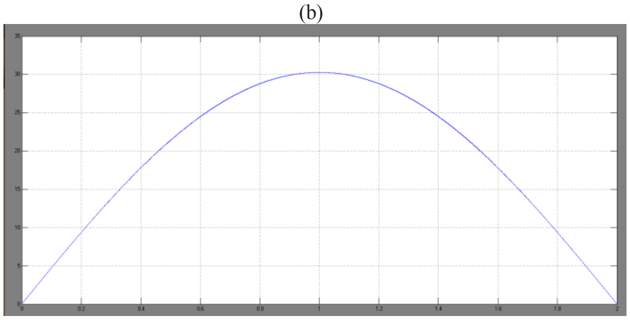

(c)

Fig 11 Simulation results using the NREL data: (a) generated PV power and (b) the dc-link voltage. (c) PV power response

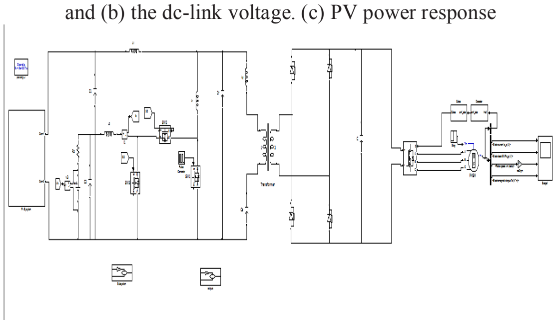

Fig 12 Matlab/simulation circuit of isolated three-port bidirectional dc–dc converter for a PV and battery system with PMSM drive

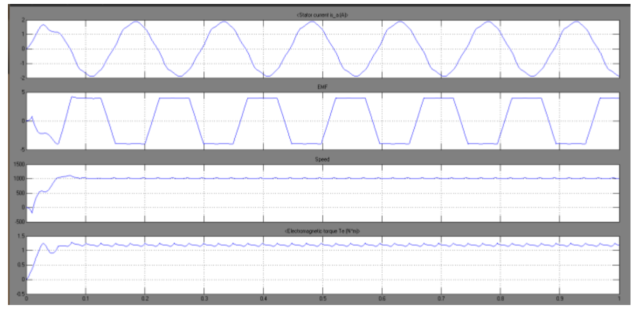

Fig 13 simulation wave form of PMSM drive stator current, EMF, speed and electromagnetic torque

VI.CONCLUSION

A high step-up three-port DC-DC converter for grid connected power systems is proposed to integrate solar and battery power. The model is developed and evaluated for different load conditions, mode change conditions etc,. The simulation results validate the functionality of the proposed converter under different solar irradiation level and load demand. Simulation results have shown that the converter is not only capable of MPPT for the PV panel when there is solar radiation but also can control the charge/discharge of the battery to maintain the dc-link voltage at a constant value. Moreover, the voltage stress and the value of di/dt of the main switch have been reduced compared with the corresponding hard-switched converter. The charging/discharging transitions of the battery could be achieved without changing the operation mode; therefore, the MPPT operation will not be interrupted. In light load condition, once the charging voltage is higher than the present level, the operation mode will be changed rapidly to protect the battery from overcharging. The outputs of the inverter is connected to the PMSM drive and study the characteristics of stator current, EMF, and speed, torque

REFERENCES

[1] C. Onwuchekwa and A. Kwasinski, “A modified-time-sharing switching technique for multiple-input DC-DC converters,” IEEE Trans. Power Electron., vol. 27, no. 11, pp. 4492–4502, Nov. 2012.

[2] A. Khaligh, J. Cao, and Y. Lee, “A multiple-input DC-DC converter topology,” IEEE Trans. Power Electron., vol. 24, no. 4, pp. 862–868, Mar. 2009.

[3] J. Lee, B. Min, D. Yoo, R. Kim, and J. Yoo, “A new topology for PV DC/DC converter with high efficiency under wide load range,” in Proc. Eur. Conf. Power Electron. Appl., Sep. 2007, pp. 1–6.

[4] C. Lohmeier, J. Zeng, W. Qiao, L. Qu, and J. Hudgins, “A currentsensorless MPPT quasi-double-boost converter for PV systems,” in Proc. IEEE Energy Convers. Congr. Expo., Sep. 2011, pp. 1069–1075.

[5] K. Sayed, M. Abdel-Salam, A. Ahmed, and M. Ahmed, “New high voltage gain dual-boost DC-DC converter for photovoltaic power system,” Elect. Power Compon. Syst., vol. 40, no. 7, pp. 711–728, Apr. 2012.

[6] Y. Chen, Y. Liu, and F. Wu, “Multi-input DC/DC converter based on the multi winding transformer for renewable energy applications,” IEEE Trans. Ind. Appl., vol. 38, no. 4, pp. 1096–1104, Jul./Aug. 2002.

[7] Y. Jang and M. Jovanovic, “Isolated boost converter,” IEEE Trans. Power Electron., vol. 22, no. 4, pp. 1514–1521, Jul. 2007.

[8] E. Yang, Y. Jiang, G. Hua, and F. Lee, “Isolated boost circuit for power factor correction,” in Proc. IEEE Appl. Power Electron. Conf. Expo., Mar. 1993, pp. 196–203.
[9] Y. Lembeye, V. Bang, G. Lefevre, and J. Ferrieux, “Novel half-bridge inductive DC-DC isolated converters for fuel cell applications,” IEEE Trans. Energy Convers., vol. 24, no. 1, pp. 203–210, Mar. 2009.
[10] J. Zeng, W. Qiao, L. Qu, and Y. Jiao, “An isolated multiport dc-dc converter for simultaneous power management of multiple different renewable energy sources,” IEEE J. Emerging Sel. Topics Power Electron., vol. 2, no. 1, pp. 70–78, Mar. 2014.
[11] H. Tao, A. Kotsopoulos, J. Duarte, and M. Hendrix, “Family of multiport bidirectional DC-DC converters,” Proc. Inst. Elect. Eng.—Elect. Power Appl., vol. 153, no. 3, pp. 451–458, May 2006.
[12] C. Zhao, S. Round, and J. Kolar, “An isolated three-port bidirectional DC-DC converter with decoupled power flow management,” IEEE Trans. Power Electron., vol. 23, no. 5, pp. 2443–2453, Sep. 2008.
[13] J. Duarte, M. Hendrix, and M. Simoes, “Three-port bidirectional converter for hybrid fuel cell systems,” IEEE Trans. Power Electron., vol. 22, no. 2, pp. 480–487, Mar. 2007.